Flow-Induced Vibration and Heat Transfer Characteristics of Two Tandem Cylinders in Different Spacing Ratios#

Haoyu He [1,2], Lin Ding[1,2, *], Yue Sun [1,2], Tian Song [1,2]

1 Key Laboratory of Low-grade Energy Utilization Technologies and Systems of Ministry of Education of China, Chongqing University, Chongqing, China

2 School of Energy and Power Engineering, Chongqing University, Chongqing, China
(Corresponding Author: linding@cqu.edu.cn)

ABSTRACT

The vibration and heat transfer characteristics of two tandem cylinders with two degrees of freedom at different reduced velocities(U^*) and spacing ratios were numerically investigated. The amplitude, trajectory, time averaged Nusselt number, vortex shedding, and temperature fields were analyzed. Results show that the dimensionless amplitudes of the two cylinders exhibited similar variation trends with increasing U^*, first increasing and then decreasing. The trajectories of both cylinders formed 8-shaped patterns. The time averaged Nusselt number (Nu_A) of cylinder 1 was higher than that of cylinder 2, and both increased with increasing U^*. The vortices shed from cylinder 1 covered the surface of cylinder 2, creating high temperature gradients and enhanced heat transfer on the surfaces of both cylinders.

Keywords: flow-induced vibration; heat transfer; Spacing ratio; two degrees of freedom vibration

NONMENCLATURE

Symbols	
c	System damping (N·s·m^{-1})
c_p	Specific heat capacity(J·kg^{-1}·K^{-1})
D	Cylinder diameter (m)
F_l	Lift (N)
F_d	Drag(N)
$f_{n,water}$	Vibration system natural frequency (s^{-1})
k	Stiffness (N·m^{-1})
m	Cylinder mass (kg)
S	The center-to-center spacing between the cylinders
U_∞	Free flow velocity (m·s^{-1})
T_w	Cylinder temperature (K)
T_∞	Free flow temperature (K)
ζ	Damping ratio
ρ	Fluid density (kg·m^{-3})

U^*	Reduced velocity[$U_\infty/f_{n,water}D$]
Pr	Prandtl number [$Pr=\upsilon/a$]
Re	Reynolds number[$U_\infty D/\upsilon$]
NuL	Local Nusselt number [hD/λ]
$Nu_{L.av}$	Time-averaged local Nusselt number [$\frac{1}{\tau_c}\int_0^{\tau_c} Nu_L d\tau$]
Nu_S	Surface-averaged Nusselt number [$\frac{1}{2\pi}\int_0^{2\pi} Nu_L d\theta$]
Nu_A	Average Nusselt number [$\frac{1}{\tau_c}\int_0^{\tau_c} Nu_S d\tau$]

1. INTRODUCTION

The steam generator is one of the key components in the nuclear reactor. To improve heat transfer efficiency inside the steam generator, heat transfer components increasingly utilize high-strength materials, resulting in thinner tube walls. This makes flow-induced vibration an issue that must be addressed in reactor engineering and structural design, as it can damage the steam generator heat transfer devices and piping. Regarding research on controlling flow-induced vibration, substantial progress has been made, leading to effective vibration suppression measures [1,2]. But some investigators have deigned heat-exchanger use vibration to enhance heat-transfer [3].

Initially, scholars focused primarily on flow and heat transfer phenomena around isolated cylinders. Bharti et al. [4] used finite element methods to study the influence of the Prandtl number on forced convection heat transfer, finding that the local Nusselt number at a fixed point on the cylinder surface increased with rising Prandtl numbers. Kumar and Jayavel [5] numerical investigation showing that high blockage ratios suppressed vortex shedding and the transition from laminar to turbulent flow. The mutual interference between cylinders leads to structural dynamic responses

and heat transfer characteristics distinct from isolated cylinders [6-8]. Borazjani [9] found that cylinders in tandem arrangements have larger oscillation amplitudes and wider lock-in regions than isolated cylinders Thus, flow and heat transfer around multiple cylinders are more complex than around a single cylinder.

The tubes in heat exchangers often exist in bundled forms. Most existing studies focus on isolated cylinder or 1DOF vibrating cylinders, while this work investigates two tandem cylinders with two degrees of freedom vibration. And the effects of spacing ratio on the flow-induced vibration and heat transfer characteristics of the tandem cylinders wad explored. Analyses of the trajectory, time averaged Nusselt number, amplitude response, vortex structures, and temperature field distributions are performed.

2. 2. PHYSICAL MODELS AND NUMERICAL MODELING

2.1 Physical system

This paper numerically simulates the flow-induced vibration and heat transfer characteristics of tandem cylinders. The physical model is illustrated in Figure 1. The system contains two rigid, isothermal cylinders with diameter D. Both cylinders can oscillate freely in the x (streamwise) and y (transverse) directions. The center-to-center spacing between the cylinders is S. The upstream cylinder is named cylinder 1 and downstream cylinder is named cylinder 2. There is no rigid connection between the two cylinders, allowing each to vibrate independently. C and K represent the system's stiffness and damping coefficients, respectively.
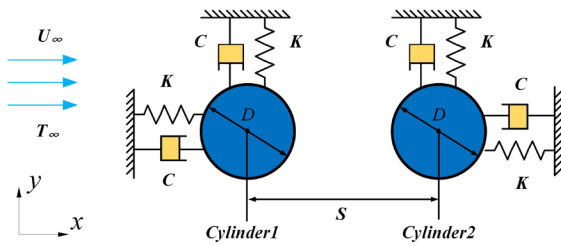
Fig. 1 Physical model schematic

2.2 Governing Equations

This study solves the two-dimensional unsteady Navier-Stokes equations to obtain the flow field. For incompressible viscous fluids, the continuity, unsteady Navier-Stokes, and energy equations are expressed as:

$$\frac{\partial u}{\partial x} + \frac{\partial v}{\partial y} = 0 \tag{1}$$

$$\frac{\partial u}{\partial t} + \frac{\partial (uu)}{\partial x} + \frac{\partial (vu)}{\partial y} = -\frac{\partial p}{\partial x} + \frac{1}{Re}\left(\frac{\partial^2 u}{\partial x^*} + \frac{\partial^2 u}{\partial y^2}\right) \tag{2}$$

$$\frac{\partial v}{\partial t} + \frac{\partial (uv)}{\partial x} + \frac{\partial (vv)}{\partial y} = -\frac{\partial p}{\partial y} + \frac{1}{Re}\left(\frac{\partial^2 v}{\partial x^2} + \frac{\partial^2 v}{\partial y^2}\right) \tag{3}$$

$$\frac{\partial \Theta}{\partial t} + \frac{\partial (u\Theta)}{\partial x} + \frac{\partial (v\Theta)}{\partial y} = \frac{1}{Pr \cdot Re}\left(\frac{\partial^2 \Theta}{\partial x^2} + \frac{\partial^2 \Theta}{\partial y^2}\right) \tag{4}$$

where u is the dimensionless velocity component in the x direction; the dimensionless time $\tau=D/U_\infty$, pressure $p=\rho U_\infty^2$, Reynolds number $Re=U_\infty D/\upsilon$, Prandtl number $Pr=\upsilon/a$, and the dimensionless temperature $\Theta=(T-T_\infty)/(T_w-T_\infty)$.

The governing equations of vibrations are:

$$\ddot{X} + \frac{4\pi\zeta}{U^*}\dot{X} + \frac{4\pi^2}{U^{*2}}X = \frac{C_d}{2m^*} \tag{5}$$

$$\ddot{Y} + \frac{4\pi\zeta}{U^*}\dot{Y} + \frac{4\pi^2}{U^{*2}}Y = \frac{C_l}{2m^*} \tag{6}$$

where $\ddot{X}$、$\dot{X}$、X ($\ddot{Y}$、$\dot{Y}$、Y) represent the dimensionless acceleration, velocity, and displacement of the cylinder in the x (and y) direction respectively. $\zeta=C/(2(Km)^{0.5})$ is the damping ratio of the system. $U^*=U_\infty/(f_{n,water}D)$ is the reduced velocity. $m^*=m/m_d$ is the mass ratio, with $m^*=1.38$ here. C_d and C_l are the drag and lift coefficients of the cylinder in the streamwise and transverse directions, respectively.

The finite volume method is used to solve fluid-thermal governing equations (Eqs. (1) ~ (4)). And the vibrating equations (Eqs. (5) ~ (6)) are calculated via forth-order Runge Kutta method. The pressure-based coupled algorithm is employed to couple pressure and velocity. The convergence is based on a scaled residual of 10^{-3} for the momentum equation and 10^{-6} for the continuity and energy equations are considered.

2.3 Computational Domain and Grid Generation

The computational domain is designed as shown in Figure 2. The dimensions of the domain are 45D×30D, with both cylinders centered in the transverse flow field. The boundary conditions are shown as Figure 2: (1) the inlet boundary is subjected to a uniform flow with constant temperature as $u = 1$ and $v = 0$, $\Theta=0$; (2) the outlet boundary is assumed as fully developed and is given as $\partial u/\partial x = \partial v/\partial x = \partial \Theta/\partial x = 0$; (3) the top and bottom boundaries are given symmetry conditions with zero heat flux $\partial u/\partial y = v = 0, \partial \Theta/\partial y = 0$; (4) the cylinder walls are having a no-slip condition with a constant temperature ($\Theta=1$).
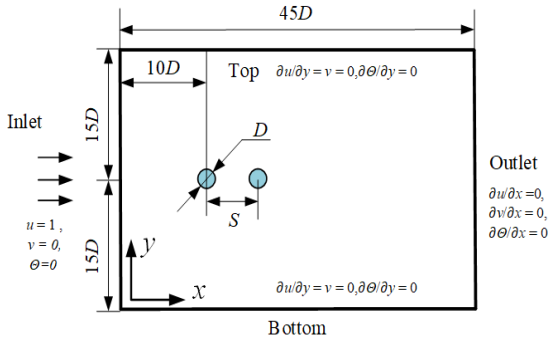
Fig. 2 Calculation domain

The Schematic diagram of mesh division is shown as Figure 3. As shown in Figure 3(a), the overset grid comprises a set of near-body grids moving with the cylinder and a set of background grids. To ensure accuracy, the interface between the cylinder's outermost grid and the background grid has similar cell sizes, as displayed in Figure 3(b) to Figure 3(d).
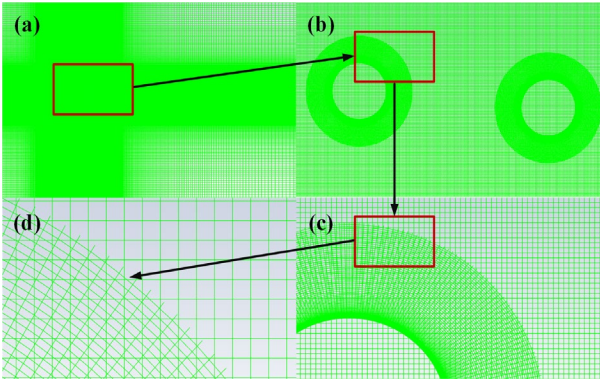
Fig. 3 Schematic diagram of mesh division (a) schematic diagram of background grid (b) (c) (d) schematic diagram of accompanying motion grid

Comparable or identical grid sizes at the cylinder-background interface help capture major flow features accurately. To validate the numerical results, a grid independence study was conducted at U^*=12, as listed in Table 1. Comparing different cases shows the maximum deviations in Nu_A between the medium grid density results and the maximum and minimum grid densities are 0.92% and 0.12%, respectively.

Table 1 Grid and computational domain independence verification (U^*=12)

Mesh quantity	A^*_m	$C_{d, mean}$	$C_{l, rms}$	Nu_A
315704+17955	0.635	1.1927	0.3599	245.7165
299088+17010	0.635	1.1927	0.3632	247.9848
265856+15120	0.635	1.1984	0.3684	248.2617

2.4 Model validation

The numerical model employed in this study has been extensively validated to predict vibration response of cylinders in our previous investigations [10-12]. The heat-transfer validation is done against the study of Izadpanah et al. [13]. The comparison of the averaged Nusselt number of a 1DOF vibrating cylinder is shown in Fig. 4. The tendency of the averaged Nusselt number of the present study agrees very well with the result of Izadpanah et al. Therefore, the numerical model used in this study is sufficient to obtain vibration and heat-transfer characteristic of cylinders.

3. RESULTS AND DISCUSSION

The effect of flow velocity and the spacing ratio of tandem cylinders on the fluid-induced vibration response and heat transfer characteristics are discussed form several aspects.
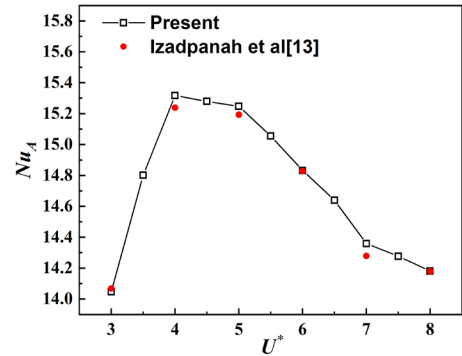
Fig. 4 The comparison of the averaged Nusselt number

3.1 Amplitude and trajectories

Figure 5 shows the dimensionless vibration amplitudes of the two cylinders in the streamwise (x) and transverse (y) direction. At a smaller spacing (S/D = 2.0), cylinder 1 has local peaks at U^* = 5 and 10. As the spacing ratio increases from 2.0 to 5.0, the maximum amplitude of cylinder 1 decreases, indicating weakened vibration. When S/D = 2.0, dimensionless amplitude of cylinder 2 changes gently from U^* = 3~9. It increases first and decreases later with rising reduced velocity, reaching the maximum at U^* = 11. When S/D = 3.0-5.0, the dimensionless amplitude trends of cylinder 1 are similar. With increasing reduced velocity, the dimensionless amplitude first increases and then decreases, reaching the maximum at U^* = 5.
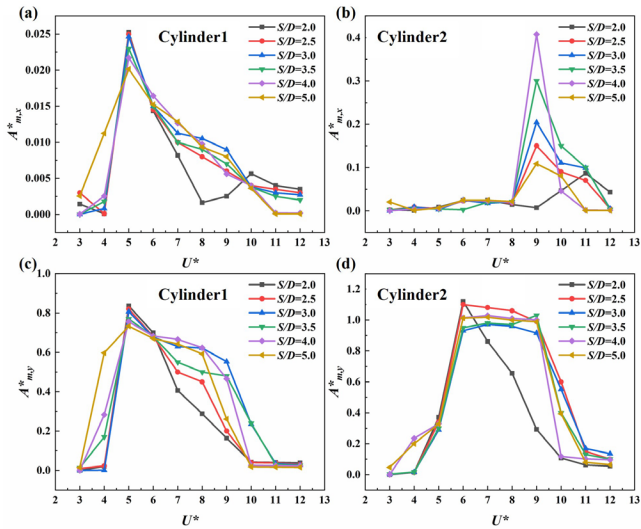
Fig.5 *Dimensionless amplitudes of two cylinders* (a) and (b) *in-line directions amplitudes,* (c) and (d) *transverse directions amplitudes*

The cylinder motions under different conditions can be visually described using trajectory plots. Figure 6 displays the trajectories of the cylinders at $U^* = 5$ for various spacing ratios. The plots show both cylinders exhibit typical 8-shaped trajectories at all spacings, resembling the digit "8". Such 8-shaped trajectories of two-degree-of-freedom FIV have also been observed in previous studies. This phenomenon arises from different oscillation frequencies and amplitudes in the x and y directions. The trajectories display amplitude of cylinder 1decreasing with increasing y spacing ratio, consistent with the trends in Figure 4. They also demonstrate the equilibrium positions of the two cylinders in the transverse (y) direction remain at $Y/D = 0$, meaning the time-averaged displacements of both cylinders stay zero. Additionally, the trajectory centers lie on the line $Y/D = 0$ for both cylinders. It can also be observed that the oscillation frequency in the streamwise direction is twice that in the transverse direction.
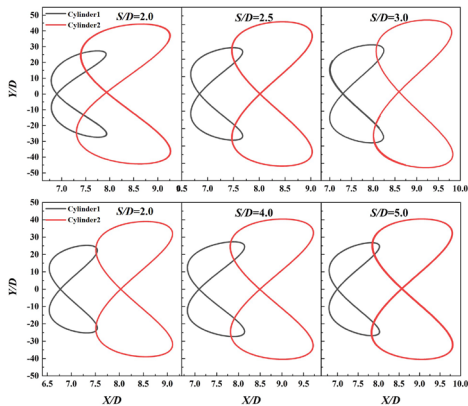
Fig.6 *Cylinder trajectory with different spacing ratios when U*=5*

3.2 *Average Nusselt number*

The variations of Nu_A with reduced velocity for both cylinders at different spacing ratios are presented in Figure 7. At same reduced velocity, the Nu_A of cylinder 1 is larger than cylinder 2. For the cylinder 2 is merged in heated wake shed from cylinder 1. The Nu_A of cylinder 1 increases with rising U^* when S/D = 2.0-5.0. At S/D = 3.0, 4.0, and 5.0, the spacing ratio has little impact on Nu_A when $U^* \geq 6$.

For cylinder 2, even though Nu_A generally rises with increasing U^*, negative Nu_A growth can occur, e.g., at U^* = 4 and 9 when S/D = 5.0. Similarly, the phenomenon of heat transfer deterioration was shown in the results of upstream fixed and downstream vibrate tandem cylinders [14]. When $U^* \geq 5$, the Nu_A trends of both cylinders versus U^* fall into two distinct groups based on the spacing ratio. Notably, the Nu_A growth rates of cylinder 1 and cylinder 2 are markedly higher at low reduced velocities than at high reduced velocities, with apparent inflection points in the growth rates. The inflection occurs at U^* = 5 for cylinder 1 and U^* = 6 for cylinder 2, indicating vibration enhanced heat transfer from the cylinders.
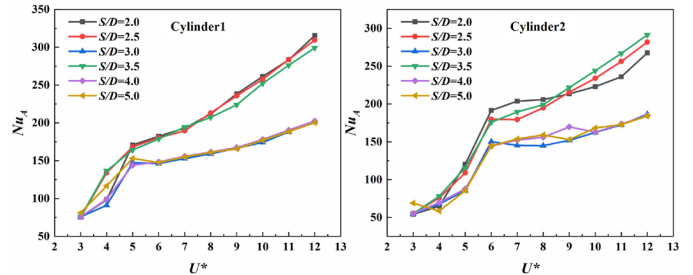
Fig.7 Averaged Nusselt number of two cylinders

3.3 *Analysis of flow field characteristics*

The cylinder wake structures, and temperature fields can effectively characterize the interaction between the upstream and downstream cylinders as well as the heat exchange between the fluid and isothermal cylinders. The wake and temperature analyses focus on U^* = 5, where vibration amplitude is large.

Figure 8 presents the wake structures of the tandem cylinders at different spacing ratios, observing the wake morphologies and mutual influence between the wakes. As cylinder 2 is downstream of cylinder 1, the vortices shed from cylinder 1 cover cylinder 2's surface. The wakes from both cylinders merge downstream into counter-rotating vortex pairs. The highest temperatures occur near the cylinder surfaces. At S/D = 3, the wake width is broadest at 5.5D.

4
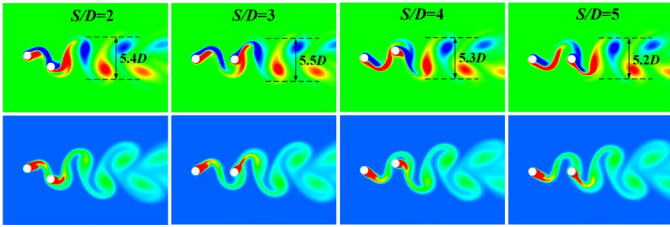
Fig.8 The vorticity and temperature field distributions

4. CONCLUSIONS

The flow-induced vibration and heat transfer characteristics of tandem cylinders with two degrees of freedom are numerically simulated. By varying the spacing ratio and reduced velocity, the streamwise and transverse dimensionless vibration amplitudes, motion trajectories, time averaged Nusselt numbers on the cylinder surfaces, wake structures, and temperature fields were discussed. The main conclusions are:

1) Spacing ratio has little influence on the vibrations of the two cylinders. At large spacings, the dimensionless amplitudes of cylinder 1 in both transverse and streamwise directions first increase and then decrease with rising U^*. Both cylinders have 8-shaped trajectories.

2) The time averaged Nusselt numbers overall rise with increasing reduced velocity. Cylinder 1 mostly has higher Nusselt numbers than cylinder 2. The Nusselt number growth is markedly higher at low reduced velocities than at high reduced velocities.

3) The vortices shed from cylinder 1 cover the surface of cylinder 2 and merge with its wake downstream. Vibrating cylinders bring high temperature gradients on their surfaces, indicating strong surface heat transfer.

4) The results will be useful to guide the design of heat-exchangers which utilize vibration to enhance heat transfer.

REFERENCE

[1] Wang, H. B., Ding, L., Zhang, L., Zou, Q. F., & Wu, C. M. Control of two-degree-of-freedom vortex-induced vibrations of a circular cylinder using a pair of synthetic jets at low Reynolds number: influence of position angle and momentum coefficient. International Journal of Heat and Fluid Flow 2019; 80, 108490.

[2] Zdravkovich, MM. Review and classification of various aerodynamic and hydrodynamic means for suppressing vortex shedding. Journal of Wind Engineering and Industrial Aerodynamics 1981; 7(2),145-189

[3] Duan, D., Ge, P., Bi, W., & Ji, J. Numerical investigation on the heat transfer enhancement mechanism of planar elastic tube bundle by flow-induced vibration. International Journal of Thermal Sciences 2017; 112, 450–459.

[4] Ram Prakash Bharti, Chhabra, R. P., & Eswaran, V. A numerical study of the steady forced convection heat transfer from an unconfined circular cylinder. Heat and Mass Transfer 2007; 43(7), 639–648

[5] Senthil kumar, R., & Jayavel, S. Influence of flow shedding frequency on convection heat transfer from bank of circular tubes in heat exchangers under cross flow. International Journal of Heat and Mass Transfer 2017; 105, 376–393.

[6] Sarpkaya, T. A critical review of the intrinsic nature of vortex-induced vibrations. Journal of Fluids and Structures 2004; 19(4), 389–447.

[7] Singh, S. P., & Mittal, S. Vortex-induced oscillations at low Reynolds numbers: Hysteresis and vortex-shedding modes. Journal of Fluids and Structures 2005; 20(8), 1085–1104.

[8] Raghavan, K., & Bernitsas, M. M.. Experimental investigation of Reynolds number effect on vortex induced vibration of rigid circular cylinder on elastic supports. Ocean Engineering 2011; 38(5), 719–731.

[9] Borazjani, I., & Sotiropoulos, F. Vortex-induced vibrations of two cylinders in tandem arrangement in the proximity–wake interference region. Journal of Fluid Mechanics 2009; 621, 321–364.

[10] Ding, L., Zhang, L., Bernitsas, M. M., & Chang, C.-C. Numerical simulation and experimental validation for energy harvesting of single-cylinder VIVACE converter with passive turbulence control. Renewable Energy 2016; 85(C), 1246–1259.

[11] Zou, Q. F., Ding, L., Wang, H. B., Wang, J., & Zhang, L. Two-degree-of-freedom flow-induced vibration of a rotating circular cylinder. Ocean Engineering 2019; 191, 106505.

[12] Wang, H. B., Ding, L., Zhang, L., Sharma, R. N., & Yang, L. Numerical study on two-degree-of-freedom vortex induced vibrations suppression of a circular cylinder via synthetic jets at different excitation frequencies. The International Journal of Heat and Fluid Flow 2020; 84, 108593.

[13] Izadpanah, E., Amini, Y., & Ashouri, A. A comprehensive investigation of vortex induced vibration effects on the heat transfer from a circular cylinder.

International Journal of Thermal Sciences 2018; 125, 405–418.

[14] Ali, U., Islam, M., & Janajreh, I. Heat transfer and wake-induced vibrations of heated tandem cylinders with two degrees of freedom: Effect of spacing ratio. Physics of Fluids 2022; 34(11).